Loss of HNF1b drives pancreatic Intraductal Papillary Mucinous Neoplasms (IPMN) initiation

Short Title: HNF1B loss promotes pancreatic IPMN onset

Diane Lorenzo,[1] Lina Aguilera Munoz,[1,2] Louis Marstrand-Daucé,[1] Anaïs Chassac,[1,3] Pascal Nicole,[1] Lingkang Meng,[1] Laurence Heidet,[4] Bertrand Knebelmann,[5] Camille Pignolet[1], Sabrina Doblas,[1] Alain Couvineau,[1] Irene Esposito,[6] Vinciane Rebours,[1,2] Rémy Nicolle,[1] Jérôme Cros,[1,7] Anne Couvelard,[1,3] Cécile Haumaitre*[1]

[1] INSERM, U1149 / Inflammation Research Center (CRI), Bichat Medical Faculty, Université Paris Cité, Paris, France.

[2] Université Paris Cité, Pancreatology and Digestive Oncology Department, Beaujon Hospital, APHP, Clichy, France.

[3] Université Paris Cité, Department of Pathology, Bichat Hospital, APHP, Paris, France.

[4] Department of Pediatric Nephrology and Reference Center for Inherited Renal Diseases (MARHEA), Necker Hospital, APHP and Université Paris Cité, Paris, France.

[5] Department of Adult Nephrology, Necker Hospital, APHP and Université Paris Cité, Paris, France.

[6] Institute of Pathology, Medical Faculty of the Heinrich Heine University, Dusseldorf, Germany.

[7] Université Paris Cité, Department of Pathology-FHU MOSAIC, Beaujon Hospital, APHP, Clichy, France.

** Corresponding author.*

cecile.haumaitre@inserm.fr

Funding

This work was supported by the Institut National de la Santé et de la Recherche Médicale (INSERM), La Ligue Contre le Cancer-Comité de Paris (grant number RS22/75-102), La fondation pour la recherche contre le cancer (ARC) (Doctoral Fellowship), the Université Paris Cité and the integrated cancer research center "SiRIC InsiTu : Insights into cancer : From inflammation to tumor" (grant number INCa-DGOS-INSERM-ITMO Cancer_18008). Part of this work was performed by a laboratory member of France Life Imaging network (grant ANR-11-INBS-0006), with the FRIM platform (UMS34).

Abbreviations

DAB: 3,3'-Diaminobenzidine; FDR: False Discovery Rate; FFPE: Formalin-fixed paraffin-embedded; GEMMs: genetically engineered mouse models; GOCC: Gene Ontology Cellular Component; GOBP: Gene Ontology Biological Process; GWAS: Genome-Wide Association Study; KEGG: Kyoto Encyclopedia of Genes and Genomes HES: Hematoxylin, Eosin, and Saffron; HGD: high-grade dysplasia; IHC: immunohistochemistry; IPMN: Intraductal Papillary Mucinous Neoplasm; LGD: low-grade dysplasia; MODY 5: maturity-onset diabetes of the young type 5; MRI: Magnetic Resonance Imaging; PanIN: Pancreatic Intraepithelial Neoplasia; PCA: Principal Component Analysis; PDAC: Pancreatic ductal adenocarcinoma; YFP: Yellow Fluorescent Protein.

Acknowledgments

We acknowledge members of the animal core facility (I. Renault, S. Olivre, A. Bouhalfaia) of the Centre de Recherche sur l'Inflammation (INSERM UMR1149). This

work benefited from equipment and services of the iGenSeq core facility at Institut du Cerveau et de la Moëlle épinière, Paris, for sequencing.

Disclosures: All authors declare no competing interests.

Data Transparency Statement: RNA sequencing datasets have been deposited in the Gene Expression Omnibus (GEO) database under accession code GSE298215.

Author Contributions

DL conceived and performed experiments, analyzed the data, obtained fundings and wrote the manuscript. LAM, LMD, An Ch, PN, LM, performed experiments and analyzed data. LH, BK, VR coordinated the clinical cohorts. SD performed MRI acquisition and analysis. IE shared methylation database. CP, Al Co, RN contributed to the sequencing experiment analyses. JC, AC analyzed data. CH designed the study, supervised the project, conceived and performed experiments, analyzed the data, obtained fundings and wrote the manuscript. All authors reviewed and approved the manuscript.

Abstract

Background & Aims: Pancreatic Intraductal Papillary Mucinous Neoplasms (IPMN) are precancerous lesions characterized by dilated and dysplastic ducts. The molecular mechanisms underlying their initiation and progression to pancreatic adenocarcinoma are not fully elucidated. While Kras mutations are highly frequent in IPMN, activating Kras in ductal cells is not sufficient to trigger IPMN formation in mice. Here, we explore whether loss of HNF1B, a transcription factor that notably plays a pivotal role in pancreatic development, predisposes to IPMN formation.

Methods: We generated a mouse model combining *Hnf1b* inactivation and an activating KRAS mutation in pancreatic ducts (KHC). The impact of HNF1B loss on IPMN development was investigated via morphological and transcriptomic analysis in vivo and in organoids, as well as in human tissue and patient cohorts.

Results: The KHC model recapitulates the development of IPMN, characterized by ductal dilation, high proliferation, papillary architecture and mucus production. Inactivation of *Hnf1b* in combination with activated KRAS drives IPMN by promoting primary cilia loss and specific oncogenic pathways such as YAP and Wnt pathways, showing the pivotal role of ciliary disruption and the key molecular alterations in IPMN initiation. *Hnf1b*-deficient pancreatic ductal cells enter a pretumoral state marked by genomic instability and early pathway dysregulation such as PI3K-AKT pathway up-regulation prior to dysplasia. Importantly, these data correlate with human IPMN, revealing *HNF1B* silencing via promoter methylation and high prevalence of IPMNs in patients harboring *HNF1B* mutations.

Conclusion: These findings identify *HNF1B* as a tumor suppressor in the initiation of IPMN and reveal key molecular mechanisms underlying the early stages of this neoplastic process.

Keywords: HNF1B, IPMN; pancreatic cancer; pancreatic tumorigenesis, primary cilium

Introduction

Pancreatic ductal adenocarcinoma (PDAC) remains a major challenge, with its incidence doubling in Western Europe over the past 30 years and a 5-year survival of less than 10%[1]. This poor prognosis is largely due to late-stage diagnoses and limited treatment options[1]. Understanding the mechanisms of tumorigenesis is critical for early detection and improving outcomes.

PDAC arises primarily from two preneoplastic lesions: Pancreatic Intraepithelial Neoplasia (PanIN), possibly originating from acinar cells, and Intraductal Papillary Mucinous Neoplasm (IPMN), which would develop from ductal cells[2–4]. While PanINs are microscopic and undetectable by imaging, IPMNs, defined as papillary growth of pancreatic ductal cells with mucin secretion, are macroscopic lesions characterized by dilated pancreatic ducts lined by dysplastic cells[5]. They affect 5–10% of adults, with the prevalence increasing with age[5]. Although not all IPMNs progress to cancer, their unpredictable evolution requires careful monitoring[5]. Three histological subtypes—gastric, intestinal, pancreatobiliary—are identified on the basis of their epithelial morphology and mucin expression by immunostaining[5], the pancreatobiliary subtype being often associated with high-grade dysplasia (HGD) and cancer[5]. The mechanisms driving the initiation and progression of IPMNs remain poorly understood. Translational research remains limited by the lack of murine models targeting ductal cells, as most induce mutations in pancreatic progenitors instead. Thus, most models fail to accurately recapitulate human IPMN development[3,6,7]. Although KRAS mutations are present in 95% of pancreatic cancers and 90% of IPMNs[8–10], activating $KRAS^{G12D}$ in pancreatic ducts of engineered mouse models (GEMMs) has failed to induce IPMNs, even with inflammation[2]. This suggests IPMN initiation requires additional genetic or epigenetic changes.

The transcription factor HNF1B is crucial for pancreatic development and is restricted to ductal cells after birth[11,12]. *HNF1B* deregulation can have tumor suppressive or oncogenic effects[13]. *HNF1B* was identified as a susceptibility locus for pancreatic cancer through Genome-Wide Association Studies (GWAS)[14]. Our team previously reported that postnatal conditional inactivation of *Hnf1b* in mouse pancreatic ductal cells leads to cystic ducts, ductal polarity defects and increased cell proliferation[15].

We hypothesized that combining *Hnf1b* inactivation with an activating *KRAS*^{G12D} mutation might induce IPMN in mice. We then used this mouse model to elucidate the molecular pathways involved in IPMN initiation and correlated these findings with human data at both the transcriptomic and phenotypic levels, revealing the role of *HNF1B* in the initiation of human IPMNs.

Materials and Methods

GEMMs

All animal experiments followed French and European ethical guidelines and were approved by the local ethical committee and the French Ministry of Research (APAFiS N°34673). The Hnf1b$^{fl/fl}$, Sox9-CreER and R26R^{YFP} mouse lines have been described previously[12,15,16]. The LSL-Kras^{G12D} mouse line was from JAX stock #008179[17]. Inactivation of *Hnf1b* and activation of KRAS in pancreatic ducts was performed via tamoxifen-induced Cre-mediated recombination under the Sox9 promoter. The different genotypes were Hnf1b$^{fl/fl}$;R26R^{YFP} namely “H” / Sox9-creER;LSL-Kras^{G12D};Hnf1b$^{+/+}$;R26R^{YFP} namely "K" / Sox9-creER;Hnf1b$^{fl/fl}$;R26R^{YFP} namely "HC" and Sox9-creER;LSL-Kras^{G12D};Hnf1b$^{fl/fl}$;R26R^{YFP} namely "KHC". Tamoxifen was

delivered postnatally via maternal milk by injecting nursing mothers (6 mg/40g) with tamoxifen (Sigma-T5648) in corn oil (20 mg/ml) four times during the litter's first week.

Histological, immunohistochemical (IHC) and immunofluorescence analyses

Dissected pancreases were fixed in 4% buffered paraformaldehyde (pH7) for 24 hours, dehydrated, and embedded in paraffin. Four levels of 3 µm sections were prepared per slide to track ductal structures in the mice. The slides were stained with HES and Alcian blue. Immunohistochemistry was performed via the Leica 3 automated system with DAB visualization and hematoxylin counterstaining. YFP-positive recombined cells were visualized using an anti-GFP antibody and a green fluorochrome-conjugated secondary antibody. Nuclei were labeled with Hoechst. The antibodies used are listed in Supplementary Table 1. Main duct diameter was averaged from three measurements on serial sections; branch duct diameter from the three largest per pancreas. Cell proliferation was measured by Ki67 staining (% positive cells/duct), with ducts outlined in Qupath software.

Magnetic Resonance Imaging (MRI)

To identify pancreatic ducts of mice at the age of 12 weeks, T2-weighted images (2D-acquisition: multi-slice axial acquisition, in-plane resolution 200µm, slice thickness 600µm, RARE sequence, echo time 25ms, repetition time 4500ms, 4 averages; and 3D acquisition: thin slices of 250µm, RARE sequence, echo time 25ms, repetition time 2500ms, 2 averages) were acquired on a 7T Bruker PharmaScan MRI system, with a 40mm volume coil for transmission/reception (platform FRIM (UMS34), CRI, University Paris-Cité, INSERM).

Pancreatic ductal organoids

Pancreata from 12-week-old H (n=5), HC (n=4), and KHC (n=4) mice were collected, chopped into small pieces, and digested with collagenase XI (Sigma-C7657). Pancreatic ducts were manually sorted from the cell suspension and seeded into 50µl BME2 (Cultrex Basement Membrane Extract, Type 2, Biotechne, 3532-010-02) matrix with specific culture medium. Organoids were cultured for 7 days to enrich ductal cells. On day 7, organoids were fixed for histology or processed for RNA extraction (RNeasy Micro Kit, Qiagen 74004). The detailed protocol for organoid culture is provided in Supplementary Material 1.

RNA-Seq analysis of mouse samples

RNA library preparation was performed using SMARTer Stranded Total RNA-Seq Kit v3- Pico Input Mammalian. cDNA and final libraries were controlled with AGILENT Tapestation 2200 on High Sensitivity DNA chip. Sequencing was perfomed on a Novaseq X illumina using a 10B flow cell 2x100 read length, aiming for a total of 30M reads per sample. Reads were aligned with the reference genome Ensemblv107_GRCm38.75 (Mus musculus samples) via STAR, and gene expression counts were obtained via FeatureCount. Extensive analysis of the differential expression transcriptome of ductal organoids was carried out using Integrated Differential Expression and Pathway (IDEP, ShinyGO, DECAFE©). H n=5; HC n=4; KHC n=4. Detailed RNAseq analysis is provided in Supplementary Material 2. The RNA sequencing datasets generated in this study have been deposited in the Gene Expression Omnibus (GEO) database under accession code GSE298215. https://www.ncbi.nlm.nih.gov/geo/query/acc.cgi?acc=GSE298215 .

RNA-Seq analysis of human IPMN

RNA extraction was performed on microdissected Formalin-fixed paraffin-embedded (FFPE) gastric IPMN tissues using the Quick-RNA FFPE Miniprep ZYMO Kit and the Roche Millisect® AVENIO Microdissector. RNA sequencing (SMARTer Kit Takara) was conducted on surgical samples (2017-2022) from patients with gastric IPMNs with low-grade dysplasia (LGD; n=140) and high-grade dysplasia (HGD; n=39) collected in Beaujon Hospital (Clichy, France). The reads were aligned with the reference Ensemblv107_GRCh38.75 (Homo sapiens samples) via STAR, and gene expression counts were obtained via FeatureCount. Differential transcriptome analysis of gastric LG- and HG-IPMNs was performed using IDEP, ShinyGO, DECAFE. Detailed analysis is provided in Supplementary Material 2.

HNF1B immunostaining on human IPMN

FFPE tissue sections from surgical specimens (2012-2022) of human IPMN, were selected on the basis of histopathological subtyping (Beaujon Hospital). HNF1B IHC was performed using the automated Leica3 IHC slide staining system (antibodies: Sigma HPA00202089 and HPA002083) across all IPMN subtypes (n=61).

HNF1B methylation analysis

HNF1B methylation was analyzed in human pancreatic ducts, LG-IPMNs (n=32), and HG-IPMNs (n=20) of both gastric (n=32) and intestinal (n=20) subtypes. Data were obtained in collaboration with the German Cancer Research Center (I. Esposito)[8]. IDAT files were loaded into ChAMP, and data analysis was processed using the R Bioconductor package Illumina Infinium HumanMethylation27 assay (Illuminaio). *HNF1B* methylation was assessed using beta values derived from specific *HNF1B*

probes relevant to gene expression and potential epigenetic silencing mechanisms, with the results visualized in a heatmap. Methylation levels were categorized using the following thresholds of beta values: Methylated (>0.5), Unmethylated (<0.4), and Intermediate (between 0.4 and 0.5). Complementary information is provided in Supplementary Material 3.

Patient cohort with constitutive *HNF1B* mutations

To identify the presence of IPMN in patients with *HNF1B* germline mutations or deletions, all the cross-sectional images (contrast-enhanced CT scans, MRI) or endoscopic ultrasounds from patients of the Pediatric Nephrology and Adult Nephrology departments (Necker Hospital, Paris, France) were reviewed. Patient imaging studies were re-evaluated to identify those with IPMN, defined as branch-duct IPMN if a communicating cystic lesion greater than 5 mm was present, or as main duct IPMN if there was pancreatic duct dilation greater than 5 mm without obstruction[5]. This study was approved by the biomedical research ethics committee (IRB00006477).

Statistical analyses

Statistical analyses were conducted using GraphPad Prism. Data are shown as means ± standard errors of the means (SEMs). Statistical significance ($p<0.05$) was assessed using descriptive statistics, chi-square tests or Fisher's exact tests for qualitative variables, Student's t-tests with Welch correction or ANOVA for multiple comparisons. Fisher’s exact test assessed HNF1B methylation across IPMN subtypes and grades. IPMN incidence in HNF1B-mutant patients was compared to an age-matched population using Poisson regression.

RESULTS

HNF1B is epigenetically downregulated in human IPMNs

HNF1B expression in human IPMN was evaluated by immunohistochemistry. HNF1B was typically expressed in the nuclei of pancreatic ductal and centroacinar cells. A loss of HNF1B expression was observed as ductal cells acquired a dysplastic phenotype, beginning at the LGD stage (Figure 1A). A complete loss of HNF1B expression was observed across all IPMN phenotypes: gastric IPMNs with LGD (n=36) and HGD (n=5), pancreatobiliary IPMNs with HGD (n=6), and intestinal IPMNs with LGD (n=21) and HGD (n=6) (Figure 1B). These results suggest a potential role for the loss of *HNF1B* expression in the initiation of IPMNs.

As *HNF1B* mutations have not been commonly reported in human sporadic IPMN, we explored promoter methylation as a potential mechanism of gene silencing. The *HNF1B* gene had a significantly greater methylation frequency among the 52 IPMNs (unmethylated: 2 (3%), intermediate: 32 (62%) and methylated: 18 (35%)) than among the 19 normal pancreatic ducts (unmethylated: 10 (53%) and intermediate: 9 (47%) (p=1.1x10-6)) (Figure 1C). Among LG-IPMNs (n=32), 2 (6%) were unmethylated, 23 (72%) had an intermediate methylation status, and 7 (22%) were methylated. Among HG-IPMNs (n=20), 9 (45%) had an intermediate methylation status, and 11 (55%) were methylated, revealing also a higher *HNF1B* methylation frequency in HG-IPMNs than in LG-IPMNs (p=0.037). The results did not vary according to the IPMN subtype: gastric or intestinal (Supplementary Figure 1).

These findings suggest that *HNF1B* methylation is an important mechanism underlying the loss of *HNF1B* expression in human IPMNs, potentially contributing to the initiation and progression of dysplastic changes in pancreatic ductal cells.

Hnf1b inactivation in the pancreatic ducts synergizes with Kras activation to form IPMN in mice

To test if *Hnf1b* loss drives IPMN initiation, a GEMM combining *Hnf1b* inactivation and KRAS activation in pancreatic ducts (KHC line: Sox9-creER;LSL-Kras^{G12D};Hnf1b$^{fl/fl}$; R26R^{YFP}) was generated. The pancreatic ducts of K mice (Sox9-creER;LSL-Kras^{G12D};Hnf1b$^{+/+}$;R26R^{YFP}) were similar to H controls, as previously reported[3,7]. The pancreatic ducts of HC mice (Sox9-creER;Hnf1b$^{fl/fl}$;R26R^{YFP}) were slightly dilated as we showed previously[15]. Phenotypic characterization by MRI, histopathological and IHC analyses demonstrated that KHC mice developed significantly more dilation of the main pancreatic duct ($p<0.0001$) (Figure 2A-E) and branch ducts ($p<0.0001$) (Figure 2F-H) compared to controls. Ki67 quantification showed increased ductal cell proliferation in KHC mice compared with HC and controls (K, H) ($p<0.0001$) (Figure 2I, J). Only KHC ducts displayed dysplasia ($p<0.0001$) with lesions positive for Alcian blue coloration and Claudin18 IHC, an early marker of pancreatic carcinogenesis (Figure 3A-D). Dysplasia affected both the main pancreatic duct (Figure 3A-C) and branch ducts (Figure 3B-D). IPMN lesions in KHC mice were fluorescent (YFP-positive) (Figure 3E-F), including glandular neoplasms (Figure 3G-G'), confirming their ductal origin.

Together, these results highlight the synergistic requirement of *Hnf1b* inactivation and KRAS activation to induce IPMN, establishing *Hnf1b* as a tumor suppressor in IPMN.

IPMN of KHC mice exhibit features similar to human gastric IPMN

The histology of IPMNs in KHC mice resembled human gastric-type IPMNs, showing papillary architecture, glandular involvement, and columnar, mucinous cells similar to gastric foveolar cells (Figure 4A). To confirm the gastric subtype, MUC1 (a marker of

gastric and pancreatobiliary subtypes) and MUC2 (a marker of the intestinal subtype) IHC were performed (Figure 4B). As expected, KHC mouse IPMNs were MUC1-apically positive and MUC2-negative. Transcriptomic analysis (detailed below) further supported the gastric identity, showing MUC6 overexpression (marker of the gastric subtype) in KHC ductal cells (Figure 4C). This gastric identity appeared to be acquired early, even before the onset of dysplasia, as HC cells also showed overexpression of gastric chief cell markers (TFF1, TFF2, PSCA, PGC, MUC5AC)(Supplementary Figure 2)[18,19].

Unraveling the molecular mechanisms of IPMN initiation through ductal organoid model

To dissect the molecular mechanisms, ductal organoids were cultured for 7 days for RNAseq analysis (Figure 5). No significant differences were observed in the growth rates (H: n=5, HC: n=4, KHC: n=4) (Supplementary Figure 3A), but tubular structures and protrusions appeared only in KHC and HC organoids, reflecting polarity defects from *Hnf1b* deficiency[15] (Figure 5A-B; Supplementary Figure 3B-C). This kind of tubular structure has been previously documented in an *in vitro* model of ducts deficient for *Brg1*[20]. SOX9 immunostaining confirmed the ductal identity of the organoids (Supplementary Figure 3D).

Principal component analysis (PCA) revealed distinct clusters of KHC, HC and H organoids, indicating marked differences in gene expression (Figure 5C). The Venn diagram showed that 645 genes were upregulated in HC and KHC compared with the H group, representing 36% of upregulated genes in HC vs H and 68% in KHC vs H. Similarly, 277 genes were downregulated in both, accounting for 38% in HC vs H and 36% in KHC vs H. Overall, many gene changes seen in KHC were already present in

HC, with more genes upregulated in KHC than in HC (Figure 5D). As expected, *Hnf1b* expression was drastically reduced in HC and KHC ducts (Figure 5E).

Hnf1b **inactivation drives primary cilium loss, ductal dysfunction and genomic instability**

K-means clustering revealed deregulated gene clusters (Figure 5F). One cluster of downregulated genes in HC and KHC ductal cells, compared to controls, was notably linked to impaired pancreatic secretion and primary cilium function. This included reduced expression of bicarbonate secretion genes, such as *Car2* ($p<0.00001$; KHC vs H). The heatmap also highlighted upregulation of extracellular matrix genes involved in cell adhesion, migration, and growth factor signaling pathways. To identify key differentially expressed genes in HC and KHC ductal cells, a volcano plot highlighted genes with the most significant expression changes (Figure 5G-H). *Scnn1a* (subunit of sodium channel, ENaC) and *Aqp5* (water channel), a spasmolytic polypeptide-expressing metaplasia (SPEM) marker[21], were among the most significantly upregulated genes (Figure 5I). Both are key regulators of intracellular osmolarity, and their upregulation correlated with reduced bicarbonate secretion[21]. They have been shown to exert oncogenic functions in pancreatic cancer[22]. *Pcks6*, linked to tumor proliferation via the Raf-MEK1/2-ERK1/2 pathway[23], was also highly upregulated in HC and KHC ductal cells (Figure 5I). In contrast, *Kif12* was strongly downregulated, reflecting impaired primary cilia function. Ductal cells indeed harbor an immotile primary cilium, a microtubule-based organelle that protrudes from the surface of ductal cells and acts as a chemo- and mechanosensor, integrating signaling pathways[24]. Immunostaining revealed the dramatic loss of primary cilia in HC and KHC ductal cells (Figure 6A-B). GOCC and GOBP pathway analyses showed downregulation of cilia-

related genes (Figure 6C-D), including *Bbs1*, *Oscp1*, *Kif12*, *Ofd1* and HNF1B direct targets *Pkhd1* and *Cys1* (Figure 6E; Supplementary Table 2)[25]. These findings highlight the crucial impact of *Hnf1b* inactivation on ciliary integrity in HC and KHC ductal cells.

Hnf1b deficiency was linked to downregulation of pathways regulating chromatin structure, cell division, mitotic spindle function, and DNA repair (Figure 6F, Supplementary Figure 4, HC vs H). Key cell division checkpoint genes, *Tp53* (G1/S checkpoint), *Cdc25c* (G2/M checkpoint), and *Bub1* (mitotic spindle checkpoint) were significantly reduced (Figure 6G), promoting uncontrolled proliferation in HC cells. The downregulation of *Chd4*, *Ezh2*, *Parp1*, *Fancl* and *Brca1* (Figure 6H) further supported defects in chromatin organization and DNA repair mechanisms, which likely contributed to the accumulation of genetic mutations. Spatial analysis revealed increased chromosomal rearrangements in HC cells (p=0.0007) (Supplementary Figure 5), suggesting that HNF1B loss promotes genomic instability and may predispose ductal cells to tumorigenesis.

Signaling pathways driving IPMN initiation in mice and humans

KEGG pathway analysis revealed early upregulation of tumorigenic pathways in HC cells, including PI3K-AKT, RAP1, cAMP, MAPK, Ras, and JAK-STAT (Figure 7A). Pathways related to mucin-type O-glycan biosynthesis and extra-cellular matrix (ECM) interactions, linked to IPMN differentiation, were upregulated, with key genes listed in Supplementary Table 2. Additional upregulated pathways in KHC ductal cells included TGF-β, Wnt, P53, and Hedgehog (Figure 7B). Notably, P53, Hippo-YAP, and Wnt signaling were significantly higher in KHC versus HC cells, underscoring their role in dysplasia development (Figure 7C; Supplementary Figure 6). During human IPMN

tumor progression from LGD to HGD, P53, Hippo-YAP, Wnt, and ECM interaction pathways were also significantly upregulated (Figure 7D; Supplementary Figure 7). Key components like CTGF/CNN2 (Hippo-YAP) and LEF1 (Wnt/β-catenin) were overexpressed in both HC and KHC vs. control H, and in human HGD-IPMN vs. LGD-IPMN (Figure 7E).

Moreover, KHC cells showed metabolic reprogramming consistent with the Warburg effect, with increased glucose uptake and lactate production despite oxygen presence. Key genes (e.g., *Acacb*, *Fasn*, *Pparγ*, *Glut1*, *Pkm2*, *Ldha*)[26] were upregulated vs. H cells and in human HGD-IPMN vs. LGD-IPMN (Supplementary Table 3). Notably, HC cells displayed this tumor-like metabolic shift even before dysplasia emerged (Supplementary Table 3).

Therefore, HC cells exhibit upregulation of oncogenic pathways such as the PI3K-AKT pathway and metabolic reprogramming, characteristics of a pretumoral state. Moreover, P53, Hippo-YAP, and Wnt/β-catenin signaling pathways appear to be key drivers of IPMN dysplasia in both mice and humans.

Increased IPMN prevalence in *HNF1B* mutation carriers

Given that *Hnf1b* deficiency predisposes to IPMN in our mouse model, we investigated whether patients with germline heterozygous *HNF1B* mutations or deletions show higher IPMN prevalence. HNF1B-related disease includes chronic renal failure, diabetes (MODY5), and frequent pancreatic atrophy[27]. While renal cysts are a key feature of *HNF1B* mutations, pancreatic cysts, especially IPMN, remain understudied in this population.

In a cohort of 130 patients followed in the pediatric and adult nephrology departments of Necker Hospital (Paris, France), 45 (mean age 35.8±16.4 years; female n=19, 42%)

had suitable kidney imaging (MRI with T2 sequences) for IPMN screening and were included in the analysis. The 85 patients without imaging data were significantly younger, with a mean age of 19.8±16.9 years. Despite agenesis of the body and tail of the pancreas in 30 (67%) patients, 14 (31%) presented with branch-duct IPMN (Figure 7F-G). Compared with the theoretical 5% incidence of IPMN in age-matched individuals, the significantly greater occurrence of branch-duct IPMN in patients with heterozygous *HNF1B* mutations (p=2.3e-08) strongly suggests that *HNF1B* functions as a tumor suppressor gene in human IPMN initiation, as demonstrated in mice.

Discussion

In humans, we found a loss of *HNF1B* expression in IPMN, including gastric, intestinal, and pancreatobiliary subtypes. This was found as dysplasia progresses in human IPMN[28]. This loss has also been documented in a mouse model of IPMN[3]. Using the KHC mouse model, we demonstrate that HNF1B loss drives IPMN development, rather than being a consequence. Supporting this, patients with constitutive HNF1B deficiency often present IPMNs.

The mechanism behind *HNF1B* downregulation in human IPMN remains unclear. Although *HNF1B* is a known susceptibility gene for pancreatic cancer, mutations have not been commonly reported in IPMNs[8,14,19,29], likely due to its exclusion from targeted sequencing panels and its complex mutational landscape, which includes over 400 known variants (ClinVar, National Center for Biotechnology Information, U.S. National Library of Medicine)[27,30,31]. These are often associated with repeat-rich DNA regions that are prone to replication errors[32,33]. While inactivating *HNF1B* mutations have been reported in prostate, endometrial, and ovarian cancers, *HNF1B* methylation is another mechanism of gene silencing observed across various cancer types (ovarian, prostate,

kidney, biliary tract, lung, colon cancers[13,34–37]). Until now, it had not been linked to pancreatic or IPMN lesions. Our data show high rates of *HNF1B* methylation in gastric and intestinal IPMNs, increasing from 22% in LGD to 55% in HGD, and reaching 100% when intermediate methylation is included. These findings emphasize the role of *HNF1B* methylation in the development of IPMN.

In the KHC mouse model, histology, immunostaining, and transcriptomics indicate that IPMNs exhibit gastric differentiation[18,19,38]. Patients with constitutive *HNF1B* deficiency develop branch duct IPMNs, which are predominantly of the gastric subtype[38,39]. The origin of human IPMN subtypes remains debated. One hypothesis posits that gastric IPMNs are an early stage that can progress to intestinal or pancreatobiliary subtypes with worse outcomes[10,40]. Another suggests distinct ductal cell subpopulations as the origin[8,18,19,29], a view supported by recent single-cell data identifying 15 such subpopulations in mice[41]. Our findings indicate that *HNF1B* deficiency initiates gastric IPMNs in both mice and humans, which might evolve into other subtypes while retaining HNF1B loss. However, HNF1B may also play a role in invasive carcinoma at later stages[28].

The molecular mechanisms initiating IPMN remain unclear, highlighting the need for relevant models such as KHC. In humans, KRAS mutations are major drivers of pancreatic oncogenesis in both IPMNs and PanINs[10]. GNAS mutations, common in 20–75% of gastric-type IPMNs[10,19,42], promote proliferation via cAMP signaling, particularly in intestinal-type IPMNs[43]. Notably, cAMP pathway activation occurs in the KHC IPMN model even without GNAS mutations. Cre-lox animal models have established the roles of KRAS and GNAS, though most initiate lesions during embryogenesis in progenitor cells[6]. These models implicate dysregulated pathways notably JAK-STAT, MAPK-EGFR, cAMP-PKA, PI3K-AKT, TGF-β, Notch and

Hedgehog in IPMN-like lesions[3,6,7]. Recent ductal cell-specific Cre models activated postnatally have confirmed a ductal origin for IPMNs and highlighted the PI3K-AKT, MAPK, and Wnt pathways as key drivers[2,3,7]. In the KHC model, IPMNs arise exclusively from ducts. Our RNA-seq analysis of duct-derived murine IPMNs revealed essential roles for the Hippo-YAP, p53, and Wnt pathways in promoting dysplasia. In humans, progression to high-grade dysplasia involves upregulation of MAPK, PI3K-AKT, JAK-STAT, TGF-β and Notch, pathways, though data vary by IPMN subtype[8,19,42]. In a large cohort of gastric-type IPMNs, we observed similar activation of Wnt, Hippo-YAP, and p53 pathways as in the KHC model, underscoring conserved molecular mechanisms and the pivotal roles of Wnt and Hippo-YAP signaling in IPMN development.

Even before the onset of dysplasia, *Hnf1b*-deficient ductal cells displayed a pretumoral state characterized by genetic instability, oncogenic signaling and metabolic reprogramming. *HNF1B* has been identified as a tumor suppressor in various cancers, including kidney, bladder, breast, prostate, ovary, uterus, liver, and colon[13,34,37,44–46]. Germline mutations in *HNF1B* are associated with chromophobe renal cell carcinoma[46]. In PDAC, the loss of HNF1B correlates with poor survival and dedifferentiation[47,48].

The loss of primary cilia due to *HNF1B* inactivation occurred in HC cells before the onset of dysplasia, as we previously reported[15]. This loss likely contributes to early tumorigenesis, as primary cilia are important for regulating key signaling pathways such as PI3K-AKT, ERK/MAPK, Wnt and Hedgehog[49,50]. In human IPMNs, primary cilia loss also occurs early, beginning at the stage of low-grade dysplasia[51]. Loss of the primary cilium stands out as a key initiating event, disrupting crucial signaling networks

and possibly facilitating other oncogenic changes, such as chromatin deregulation and genomic instability.

Recent studies by Dhara and colleagues have shown that changes in chromatin accessibility associated with HNF1B are essential for preserving genomic integrity and preventing tumor progression[47]. In HC cells, the reduced expression of genes involved in chromatin organization may further predispose cells to transformation. RNA-sequencing of KHC cells that have progressed to dysplasia revealed a loss of ductal identity. This observation supports the concept of “ductal retrogression” previously described in Brg1-deficient ductal cells, Brg1 being a key component of the SWI/SNF chromatin remodeling complex[20]. This highlights the role of HNF1B in IPMN initiation through its involvement in chromatin regulation.

In HC cells, *Hnf1b* deficiency also results in downregulation of genes required for mitotic checkpoints, DNA repair, and spindle formation. This downregulation promotes genomic instability, mutations, and chromosomal rearrangements, contributing to the development of dysplasia[45,52]. Similar patterns of chromosomal instability are observed in chromophobe renal cancer and in patients with germline *HNF1B* mutations. In prostate cancer, the loss of *HNF1B* has been linked to reduced expression of the spindle checkpoint genes Mad2l1 and Bub1, both of which are direct transcriptional targets of HNF1B. In HC cells, chromosomal instability, including reduced expression of Mad2l1 and Bub1, is observed before the onset of dysplasia, indicating chromosomal instability is an early event[53].

Moreover, HNF1B acts as a bookmarker, maintaining the continuity of gene expression across cell divisions[54]. Loss of this function disrupts normal cell division and may contribute to tumor progression[55]. Our study also revealed that the absence of *Hnf1b* leads to decreased expression of several critical cell cycle regulators, including

caretaker tumor suppressor genes such as Tp53, Bub1, and Ezh2[56,57]. Evidence suggests that HNF1B and TP53 may act cooperatively, and their combined loss has been associated with enhanced tumor aggressiveness in kidney cancer[46,58]. Bub1 and Ezh2 have been identified as direct transcriptional targets of HNF1B in different organs[46]. Their downregulation may promote a mutagenic environment in HC cells, positioning *Hnf1b* itself as a caretaker gene. Additional genes involved in DNA repair, such as Cdc25c, Msh2, and Blm, known as direct targets of HNF1B in PDAC PANC1 cells (Chip-Atlas Consortium; 2024) were also significantly downregulated in HC ducts.

Taken together, these results establish HNF1B as a tumor suppressor gene involved in the initiation of IPMNs. This is supported by the frequent loss of HNF1B expression observed in human IPMNs, primarily due to gene silencing through promoter methylation, and by the high prevalence of IPMNs in patients carrying constitutive HNF1B mutations. Mechanistically, the loss of HNF1B predisposes pancreatic cells to tumorigenesis through disrupted primary cilia, chromatin remodeling, genomic instability, impaired cell cycle regulation and activation of specific oncogenic signaling pathways. These findings clarify the molecular events driving early IPMN development and also have clinical implications for the monitoring of individuals with HNF1B syndrome. They also highlight potential therapeutic strategies, such as restoring HNF1B expression, reestablishing ciliary function, or targeting the YAP and Wnt pathways.

References

1. Siegel RL, Miller KD, Jemal A. Cancer statistics, 2019. CA Cancer J Clin 2019;69:7–34.

2. Kopp JL, Figura G von, Mayes E, et al. Identification of Sox9-dependent acinar-to-ductal reprogramming as the principal mechanism for initiation of pancreatic ductal adenocarcinoma. Cancer Cell 2012;22:737–750.

3. Collet L, Ghurburrun E, Meyers N, et al. Kras and Lkb1 mutations synergistically induce intraductal papillary mucinous neoplasm derived from pancreatic duct cells. Gut 2020;69:704–714.

4. Marstrand-Daucé L, Lorenzo D, Chassac A, et al. Acinar-to-Ductal Metaplasia (ADM): On the Road to Pancreatic Intraepithelial Neoplasia (PanIN) and Pancreatic Cancer. Int J Mol Sci 2023;24:9946.

5. Ohtsuka T, Fernandez-del Castillo C, Furukawa T, et al. International evidence-based Kyoto guidelines for the management of intraductal papillary mucinous neoplasm of the pancreas. Pancreatology 2023:S1424390323018835.

6. Li J, Wei T, Zhang J, et al. Intraductal Papillary Mucinous Neoplasms of the Pancreas: A Review of Their Genetic Characteristics and Mouse Models. Cancers 2021;13:5296.

7. Kopp JL, Dubois CL, Schaeffer DF, et al. Loss of Pten and Activation of Kras Synergistically Induce Formation of Intraductal Papillary Mucinous Neoplasia From Pancreatic Ductal Cells in Mice. Gastroenterology 2018;154:1509-1523.e5.

8. Liffers S-T, Godfrey L, Frohn L, et al. Molecular heterogeneity and commonalities in pancreatic cancer precursors with gastric and intestinal phenotype. Gut 2023;72:522–534.

9. Lee J-H, Kim Y, Choi J-W, et al. KRAS, GNAS, and RNF43 mutations in intraductal papillary mucinous neoplasm of the pancreas: a meta-analysis. SpringerPlus 2016;5:1172.

10. Fischer CG, Beleva Guthrie V, Braxton AM, et al. Intraductal Papillary Mucinous Neoplasms Arise From Multiple Independent Clones, Each With Distinct Mutations. Gastroenterology 2019;157:1123-1137.e22.

11. Haumaitre C, Barbacci E, Jenny M, et al. Lack of TCF2/vHNF1 in mice leads to pancreas agenesis. Proc Natl Acad Sci U S A 2005;102:1490–1495.

12. De Vas MG, Kopp JL, Heliot C, et al. Hnf1b controls pancreas morphogenesis and the generation of Ngn3+ endocrine progenitors. Dev Camb Engl 2015;142:871–882.

13. Chandra S, Srinivasan S, Batra J. Hepatocyte nuclear factor 1 beta: A perspective in cancer. Cancer Med 2021;10:1791–1804.

14. Klein AP, Wolpin BM, Risch HA, et al. Genome-wide meta-analysis identifies five new susceptibility loci for pancreatic cancer. Nat Commun 2018;9:556.

15. Quilichini E, Fabre M, Dirami T, et al. Pancreatic Ductal Deletion of Hnf1b Disrupts Exocrine Homeostasis, Leads to Pancreatitis, and Facilitates Tumorigenesis. Cell Mol Gastroenterol Hepatol 2019;8:487–511.

16. Kopp JL, Dubois CL, Schaffer AE, et al. Sox9+ ductal cells are multipotent progenitors throughout development but do not produce new endocrine cells in the normal or injured adult pancreas. Development 2011;138:653–665.

17. Jackson EL, Willis N, Mercer K, et al. Analysis of lung tumor initiation and progression using conditional expression of oncogenic *K-ras*. Genes Dev 2001;15:3243–3248.

18. Sans M, Makino Y, Min J, et al. Spatial Transcriptomics of Intraductal Papillary Mucinous Neoplasms of the Pancreas Identifies NKX6-2 as a Driver of Gastric Differentiation and Indolent Biological Potential. Cancer Discov 2023;13:1844–1861.

19. Agostini A, Piro G, Inzani F, et al. Identification of spatially-resolved markers of malignant transformation in Intraductal Papillary Mucinous Neoplasms. Nat Commun 2024;15:2764.

20. Roy N, Malik S, Villanueva KE, et al. Brg1 promotes both tumor-suppressive and oncogenic activities at distinct stages of pancreatic cancer formation. Genes Dev 2015;29:658–671.

21. Lee S-H, Jang B, Min J, et al. Up-regulation of Aquaporin 5 Defines Spasmolytic Polypeptide-Expressing Metaplasia and Progression to Incomplete Intestinal Metaplasia. Cell Mol Gastroenterol Hepatol 2022;13:199–217.

22. Gao F, Wang D, Liu X, et al. Sodium channel 1 subunit alpha SCNN1A exerts oncogenic function in pancreatic cancer via accelerating cellular growth and metastasis. Arch Biochem Biophys 2022;727:109323.

23. He H, Zhang S, Yang H, et al. Identification of Genes Associated with Liver Metastasis in Pancreatic Cancer Reveals PCSK6 as a Crucial Mediator. Cancers 2022;15:241.

24. Lodh S, O'Hare EA, Zaghloul NA. Primary cilia in pancreatic development and disease. Birth Defects Res Part C Embryo Today Rev 2014;102:139–158.

25. Van Dam TJP, Kennedy J, Van Der Lee R, et al. CiliaCarta: An integrated and validated compendium of ciliary genes Stieger K, ed. PLOS ONE 2019;14:e0216705.

26. Lu C-W, Lin S-C, Chen K-F, et al. Induction of Pyruvate Dehydrogenase Kinase-3 by Hypoxia-inducible Factor-1 Promotes Metabolic Switch and Drug Resistance. J Biol Chem 2008;283:28106–28114.

27. Gambella A, Kalantari S, Cadamuro M, et al. The Landscape of HNF1B Deficiency: A Syndrome Not Yet Fully Explored. Cells 2023;12:307.

28. Kato H, Tateishi K, Fujiwara H, et al. MNX1-HNF1B Axis Is Indispensable for Intraductal Papillary Mucinous Neoplasm Lineages. Gastroenterology 2022;162:1272-1287.e16.

29. Michiels E, Madhloum H, Van Lint S, et al. High-resolution and quantitative spatial analysis reveal intra-ductal phenotypic and functional diversification in pancreatic cancer. J Pathol 2024;262:76–89.

30. Nikiforova MN, Wald AI, Spagnolo DM, et al. A Combined DNA/RNA-based Next-Generation Sequencing Platform to Improve the Classification of Pancreatic Cysts and

Early Detection of Pancreatic Cancer Arising From Pancreatic Cysts. Ann Surg 2023;278:e789–e797.

31. Paniccia A, Polanco PM, Boone BA, et al. Prospective, Multi-Institutional, Real-Time Next-Generation Sequencing of Pancreatic Cyst Fluid Reveals Diverse Genomic Alterations That Improve the Clinical Management of Pancreatic Cysts. Gastroenterology 2023;164:117-133.e7.

32. Durrett R. Basic Models. In: *Probability Models for DNA Sequence Evolution*. Probability and its Applications. New York, NY: Springer New York; 2008:1–52.

33. Matsuda T, Bebenek K, Masutani C, et al. Low fidelity DNA synthesis by human DNA polymerase-η. Nature 2000;404:1011–1013.

34. Ross-Adams H, Ball S, Lawrenson K, et al. *HNF1B* variants associate with promoter methylation and regulate gene networks activated in prostate and ovarian cancer. Oncotarget 2016;7:74734–74746.

35. Dundr P, Bártů M, Hojný J, et al. HNF1B, EZH2 and ECI2 in prostate carcinoma. Molecular, immunohistochemical and clinico-pathological study. Sci Rep 2020;10:14365.

36. Bártů M, Hojný J, Hájková N, et al. Analysis of expression, epigenetic, and genetic changes of HNF1B in 130 kidney tumours. Sci Rep 2020;10:17151.

37. Bártů M, Hojný J, Hájková N, et al. Expression, Epigenetic, and Genetic Changes of HNF1B in Colorectal Lesions: an Analysis of 145 Cases. Pathol Oncol Res 2020;26:2337–2350.

38. Furukawa T. Subtyping of IPMN. Methods Mol Biol Clifton NJ 2019;1882:1–8.

39. Ishida M, Egawa S, Aoki T, et al. Characteristic Clinicopathological Features of the Types of Intraductal Papillary-Mucinous Neoplasms of the Pancreas: Pancreas 2007;35:348–352.

40. Omori Y, Ono Y, Tanino M, et al. Pathways of Progression From Intraductal Papillary Mucinous Neoplasm to Pancreatic Ductal Adenocarcinoma Based on Molecular Features. Gastroenterology 2019;156:647-661.e2.

41. Fernández Á, Casamitjana J, Holguín-Horcajo A, et al. A Single-Cell Atlas of the Murine Pancreatic Ductal Tree Identifies Novel Cell Populations With Potential Implications in Pancreas Regeneration and Exocrine Pathogenesis. Gastroenterology 2024:S0016508524050637.

42. Felsenstein M, Noë M, Masica DL, et al. IPMNs with co-occurring invasive cancers: neighbours but not always relatives. Gut 2018;67:1652–1662.

43. Patra KC, Kato Y, Mizukami Y, et al. Mutant GNAS drives pancreatic tumourigenesis by inducing PKA-mediated SIK suppression and reprogramming lipid metabolism. Nat Cell Biol 2018;20:811–822.

44. Nie C, Wang B, Wang B, et al. Integrative Analysis of HNF1B mRNA in Human Cancers Based on Data Mining. Int J Med Sci 2020;17:2895–2904.

45. Lu W, Sun J, Zhou H, et al. HNF1B inhibits cell proliferation via repression of SMAD6 expression in prostate cancer. J Cell Mol Med 2020;24:14539–14548.

46. Sun M, Tong P, Kong W, et al. HNF1B Loss Exacerbates the Development of Chromophobe Renal Cell Carcinomas. Cancer Res 2017;77:5313–5326.

47. Dhara S, Chhangawala S, Chintalapudi H, et al. Pancreatic cancer prognosis is predicted by an ATAC-array technology for assessing chromatin accessibility. Nat Commun 2021;12:3044.

48. Bai S, Lindberg J, Whalen G, et al. Utility of HNF-1B and a panel of lineage-specific biomarkers to optimize the diagnosis of pancreatic ductal adenocarcinoma. Am J Cancer Res 2021;11:858–865.

49. Higgins M, Obaidi I, McMorrow T. Primary cilia and their role in cancer (Review). Oncol Lett 2019.

50. Gradilone SA, Pisarello MJ, LaRusso NF. Primary Cilia in Tumor Biology: The Primary Cilium as a Therapeutic Target in Cholangiocarcinoma. Curr Drug Targets 2017;18:958–963.

51. Schimmack S, Kneller S, Dadabaeva N, et al. Epithelial to Stromal Re-Distribution of Primary Cilia during Pancreatic Carcinogenesis Rooman I, ed. PLOS ONE 2016;11:e0164231.

52. Giam M, Rancati G. Aneuploidy and chromosomal instability in cancer: a jackpot to chaos. Cell Div 2015;10:3.

53. Negrini S, Gorgoulis VG, Halazonetis TD. Genomic instability — an evolving hallmark of cancer. Nat Rev Mol Cell Biol 2010;11:220–228.

54. Lerner J, Bagattin A, Verdeguer F, et al. Human mutations affect the epigenetic/bookmarking function of HNF1B. Nucleic Acids Res 2016;44:8097–8111.

55. Zaidi SK, Grandy RA, Lopez-Camacho C, et al. Bookmarking Target Genes in Mitosis: A Shared Epigenetic Trait of Phenotypic Transcription Factors and Oncogenes? Cancer Res 2014;74:420–425.

56. Levitt NC, Hickson ID. Caretaker tumour suppressor genes that defend genome integrity. Trends Mol Med 2002;8:179–186.

57. Duan R, Du W, Guo W. EZH2: a novel target for cancer treatment. J Hematol OncolJ Hematol Oncol 2020;13:104.

58. Haili L, Yongjin Z, Juhua D, et al. p53 mutation regulates PKD genes and results in co-occurrence of PKD and tumorigenesis. Cancer Biol Med 2019;16:79.

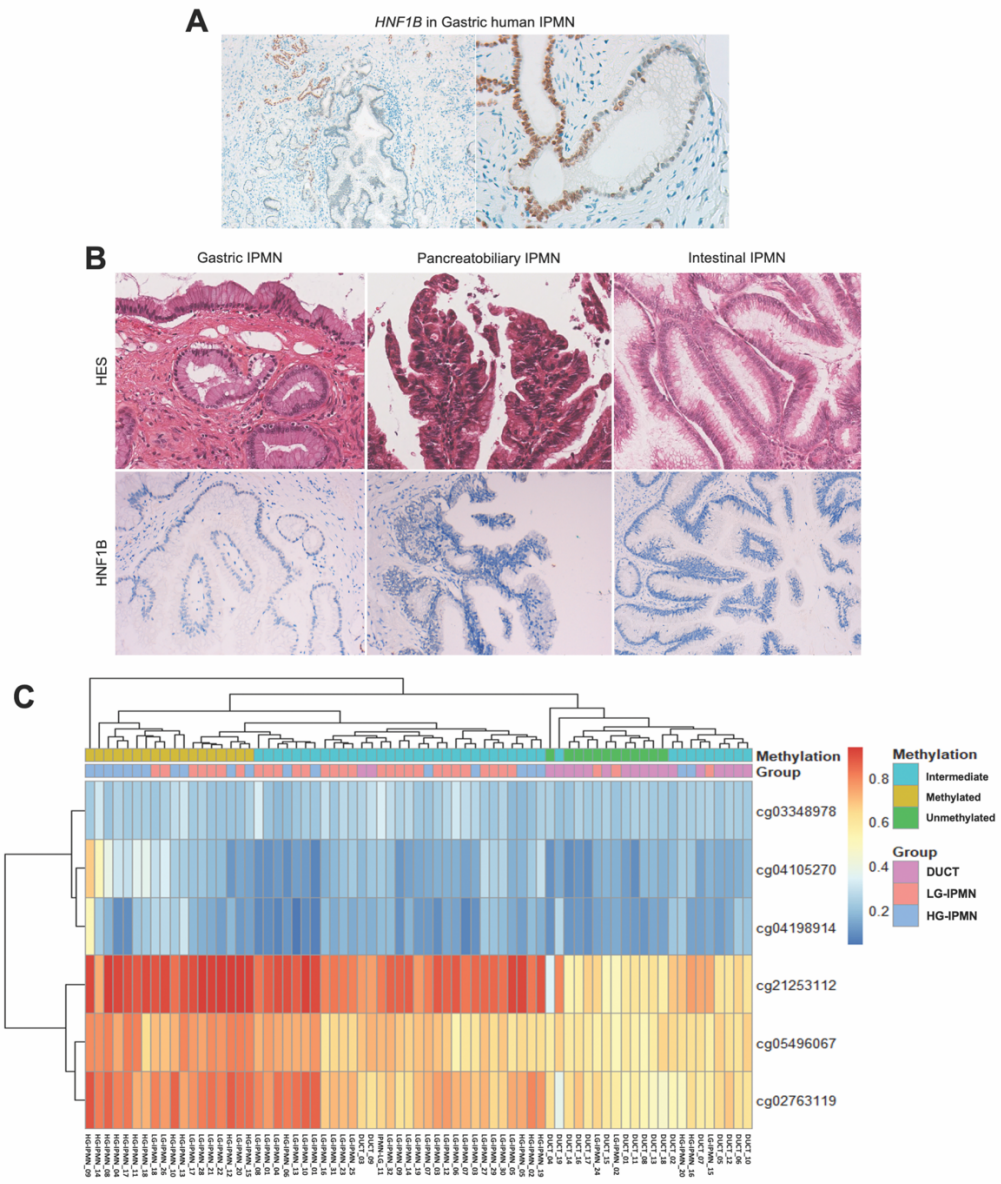

Figure 1: Loss of HNF1B expression in human IPMN

(A) HNF1B immunostaining of human gastric-IPMN showing positive HNF1B staining in ductal cells and negative expression in human gastric IPMN. Right panel: Progressive loss of HNF1B expression with the onset of dysplasia. (B) HES staining and HNF1B immunostaining of human IPMN showing HNF1B extinction in dysplastic cells. (C) Mean CpG methylation of HNF1B probes known to modulate HNF1B expression in human ducts (n=19), gastric (n=32) and intestinal (n=20) IPMN, LG-IPMN (n=32) and HG-IPMN (n=20) (unmethylated: mean β-value <0.4; intermediate: mean β-value >0.4 and <0.5; methylated: mean β-value >0.5). Scale bar, 100 µm.

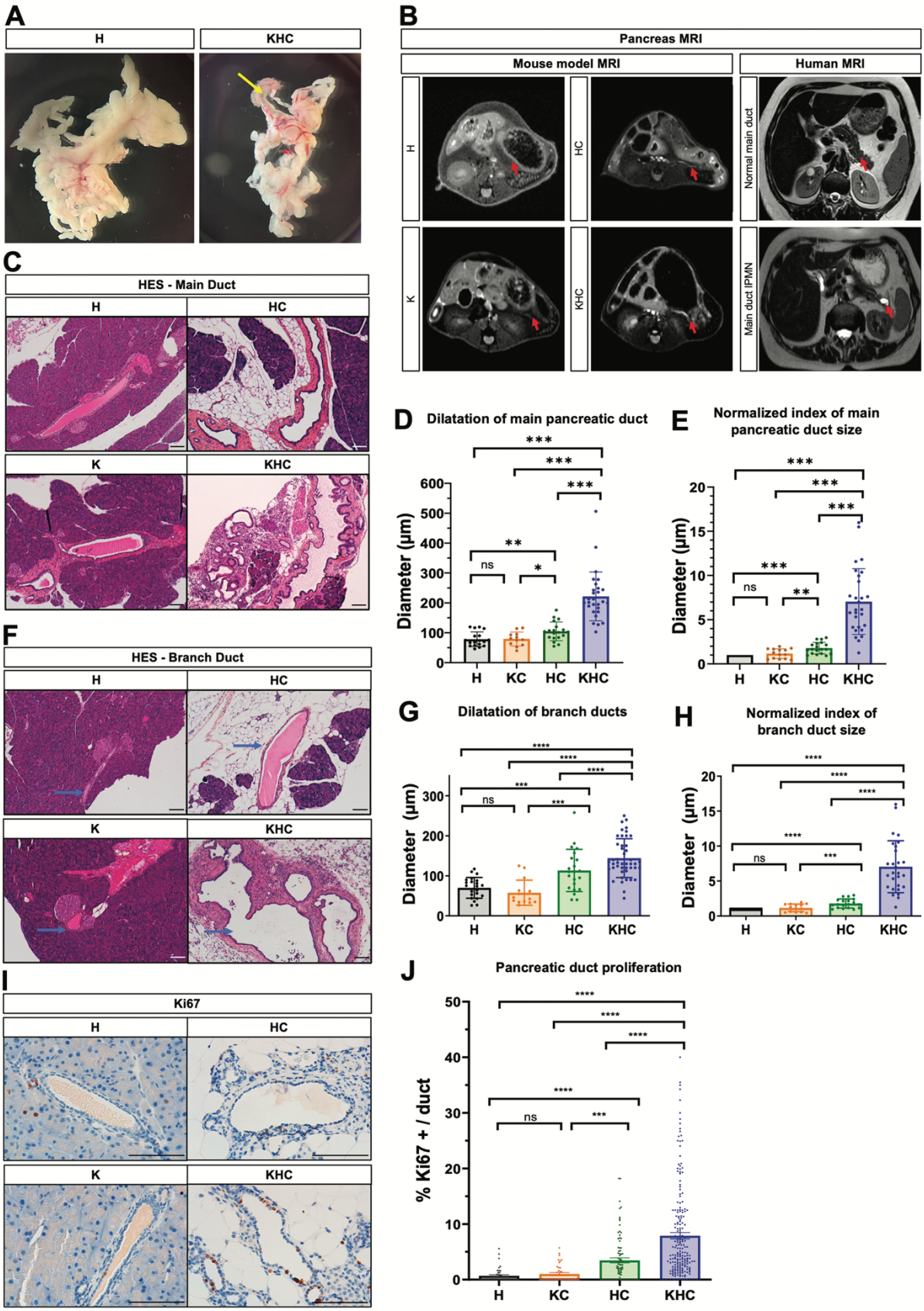
A
H
KHC
B
Pancreas MRI
Mouse model MRI
Human MRI
H
HC
Normal main duct
K
KHC
Main duct IPMN
C
HES - Main Duct
H
HC
K
KHC
D
Dilatation of main pancreatic duct
Diameter (µm)
H
KC
HC
KHC
E
Normalized index of main pancreatic duct size
Diameter (µm)
F
HES - Branch Duct
G
Dilatation of branch ducts
H
Normalized index of branch duct size
I
Ki67
J
Pancreatic duct proliferation
% Ki67 + / duct

Figure 2: Pancreatic duct morphology and proliferation in KHC mice compared with controls

(A) Pancreatic tissue from H and KHC mice. KHC mice show main duct dilation (yellow arrow) and bulging branch ducts, with reduced parenchyma. (B) T2-weighted MRI of mice (left) and human (right). The main pancreatic duct is absent in H and K mice, faintly visible in HC, and dilated in KHC mice. Human images show a normal duct (top right) and a moniliform dilation in the pancreatic tail consistent with IPMN (bottom right). (C) HES-stained histological section of the main pancreatic duct. (D) Diameters of the main pancreatic duct show greater dilation in KHC (n=28) compared to HC (n=19), K (n=12) and H (n=18) mice. (E) Index of main pancreatic duct size (duct dilation normalized to pancreas weight, with control set at 1). The KHC main pancreatic duct was 7 times more dilated than H, and the HC was 2 times more dilated than H. (F) HES-stained histological section of pancreatic secondary duct (blue arrow). (G) Diameters of branch pancreatic ducts show greater dilation of the secondary duct in KHC (n=45) mice compared to HC (n=22), K (n=15) and H (n=22). (H) Index of branch ducts (branch duct dilation normalized to pancreas weight, with control set at 1), reveals 7-fold greater dilation in KHC mice compared to H mice, with a 2-fold increase observed in HC compared to H. (I) Ki67 IHC of pancreatic ducts from KHC, HC, K and H mice. (J) Quantification of pancreatic ductal proliferation. Number of ducts counted H (n=43), HC (n=87), K (n=41) and KHC (n=211). * $p<0.01$, ** $p<0.001$, *** $p<0.0001$ and **** $p<0,00001$. Genotypes of the mice: "H" Hnf1b$^{fl/fl}$;R26R^{YFP}, "K" Sox9-cre^{ER};LSL-Kras^{G12D};Hnf1b$^{+/+}$;R26R^{YFP}, "HC" Sox9-cre^{ER};Hnf1b$^{fl/fl}$;R26R^{YFP}, "KHC" Sox9-cre^{ER};LSL-Kras^{G12D};Hnf1b$^{fl/fl}$;R26R^{YFP}.

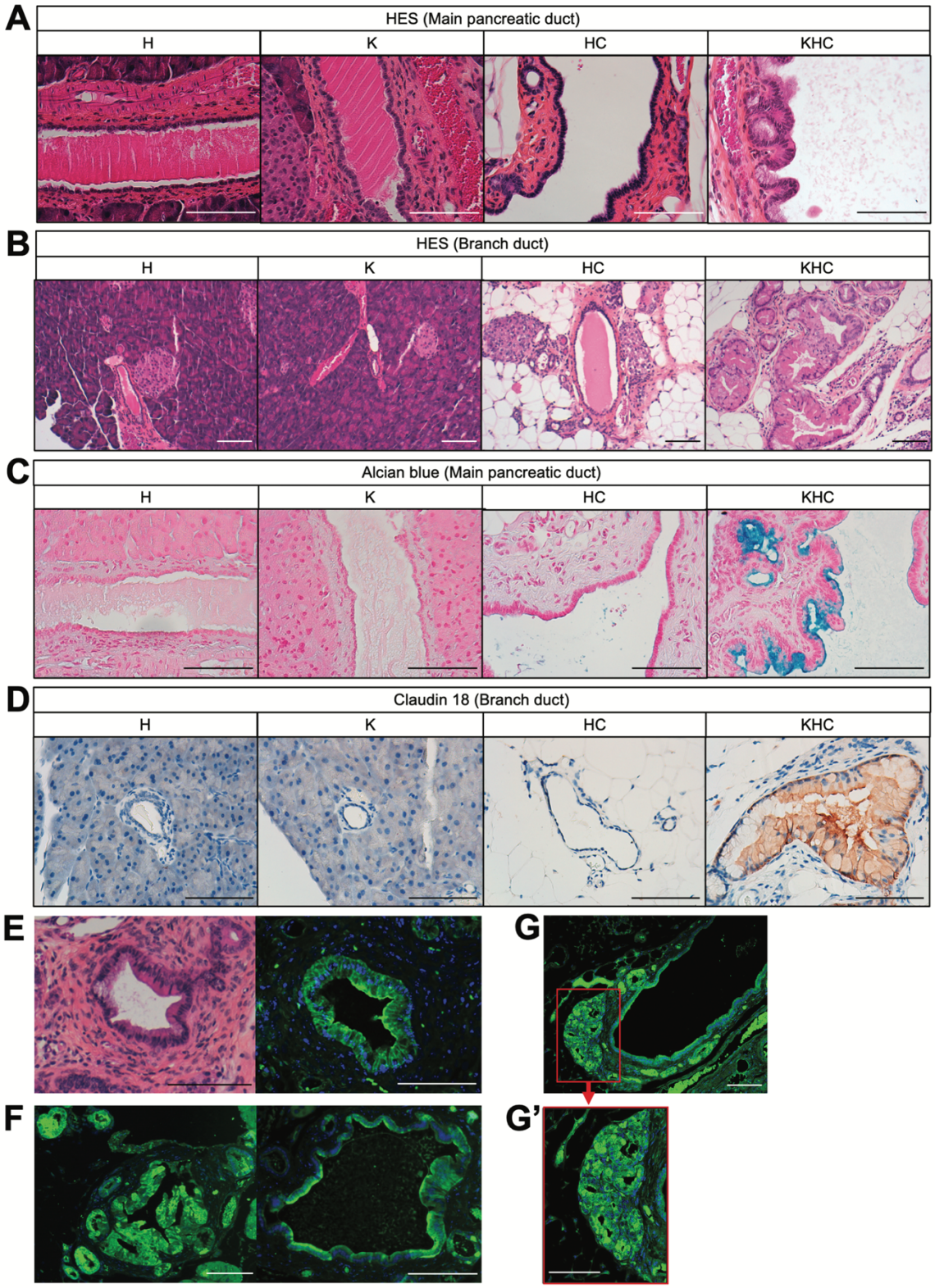

Figure 3: Histological and immunofluorescence characterization of pancreatic ductal lesions in KHC mutants compared with HC, K and H mice

(A) HES staining of the main pancreatic duct of H, K, HC and KHC. (B) HES staining of the branch ducts of H, K, HC and KHC. (C) Alcian blue coloration (mucus presence) of KHC lesion in the main pancreatic duct. (D) Immunohistochemical staining of Claudin-18 showing positive labeling of the KHC lesion in a branch duct. KHC mice exhibit dysplastic lesions with papillary formation, swollen cytoplasm, nuclear deformation, and mucus production, all positively labeled with Claudin 18. (E) HES staining of a ductal dysplasia lesion of a branch duct (left panel) and YFP-immunofluorescence (right panel), highlighting IPMN branch-duct cell lineage in KHC mice. Nuclei labeled with Hoechst. (F) Dysplastic papillary lesion of the main pancreatic duct showing YFP-immunofluorescence within dysplasia. (G, G') YFP-immunofluorescence of a main pancreatic duct from KHC mice with an enlarged glandular neoplasm, showing its ductal identity. Nuclei labeled with Hoechst. Scale bar, 100 μm.

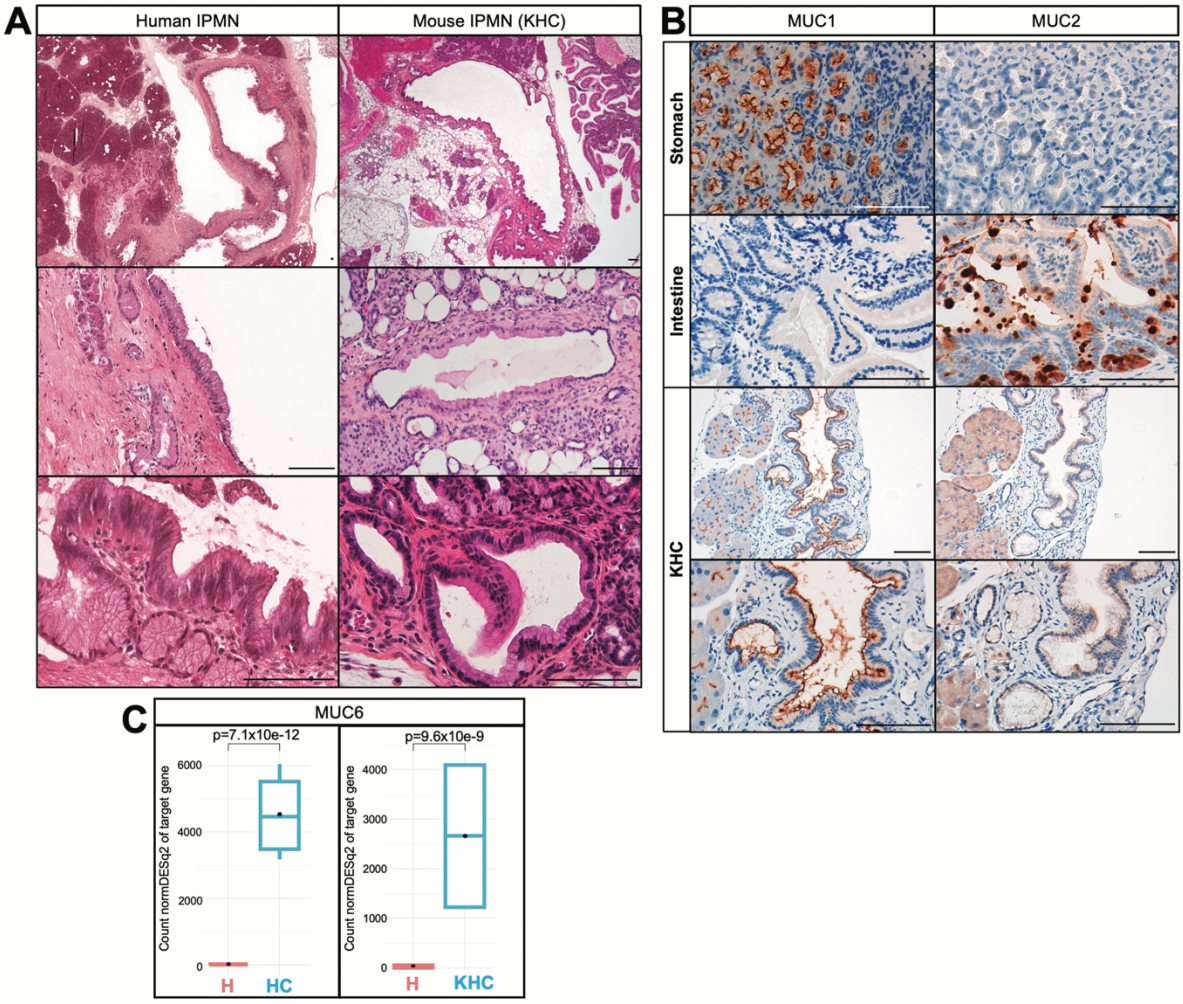

Figure 4: Gastric subtype of murine KHC IPMN

(A) HES staining of human gastric IPMN and KHC mice IPMN showing histological similarities, with columnar-shaped cells and mucinous neoplasms. (B) MUC1 and MUC2 IHC of KHC mice IPMN, with mouse stomach as a positive control for MUC1 immunostaining and mouse intestine as a positive control for MUC2 immunostaining. (C) Boxplot of MUC6 expression, showing MUC6 upregulation in HC and KHC ducts compared to H. Scale bar, 100 µm.

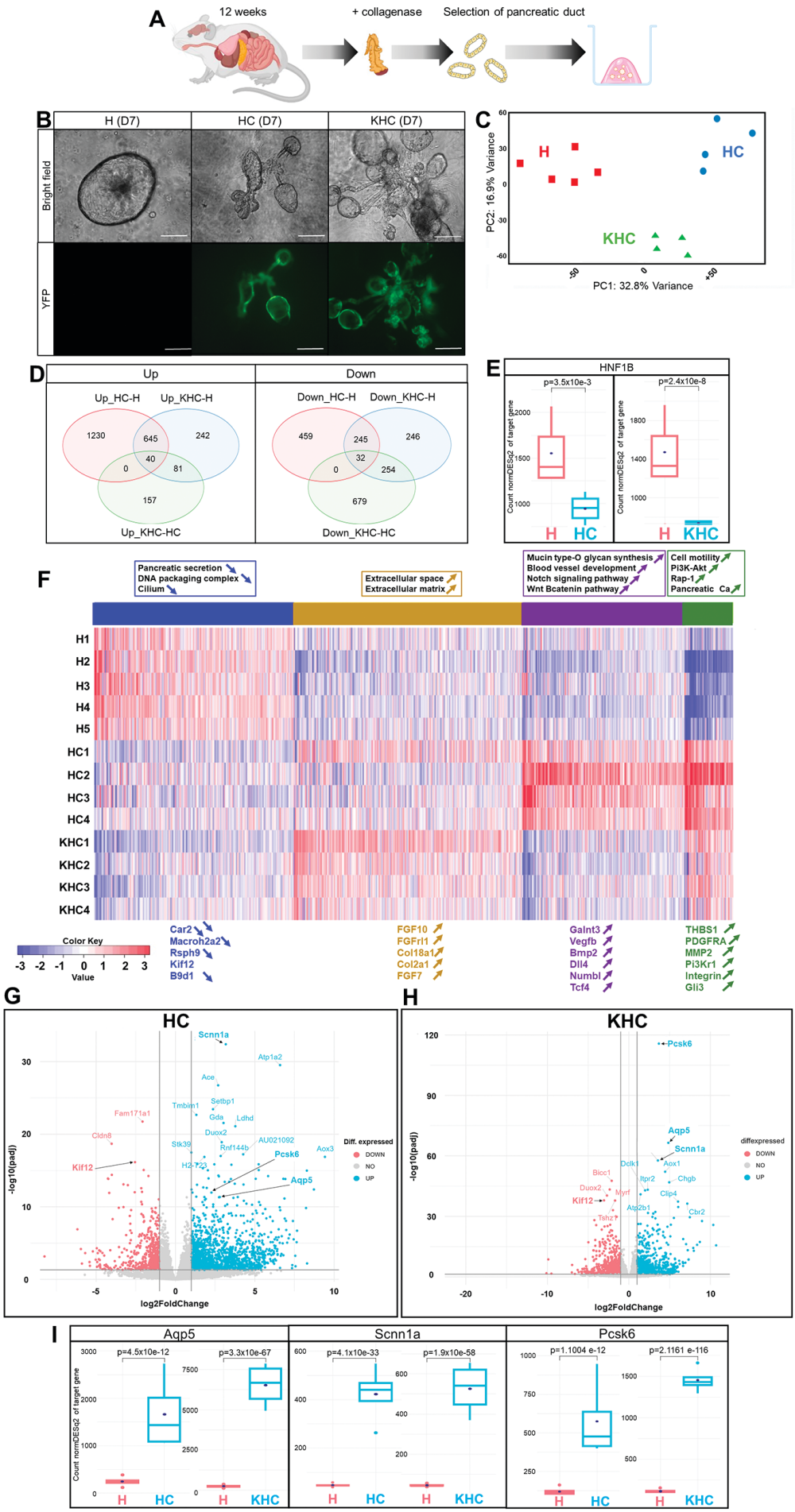
A
12 weeks
+ collagenase
Selection of pancreatic duct
B
H (D7)
HC (D7)
KHC (D7)
Bright field
YFP
C
PC2: 16.9% Variance
PC1: 32.8% Variance
H
HC
KHC
D
Up
Down
Up_HC-H
Up_KHC-H
Up_KHC-HC
Down_HC-H
Down_KHC-H
Down_KHC-HC
E
HNF1B
p=3.5x10e-3
p=2.4x10e-8
Count normDESq2 of target gene
H
HC
KHC
F
Pancreatic secretion
DNA packaging complex
Cilium
Extracellular space
Extracellular matrix
Mucin type-O glycan synthesis
Blood vessel development
Notch signaling pathway
Wnt Bcatenin pathway
Cell motility
Pi3K-Akt
Rap-1
Pancreatic Ca
H1
H2
H3
H4
H5
HC1
HC2
HC3
HC4
KHC1
KHC2
KHC3
KHC4
Color Key
Value
Car2
Macroh2a2
Rsph9
Kif12
B9d1
FGF10
FGFrl1
Col18a1
Col2a1
FGF7
Galnt3
Vegfb
Bmp2
Dll4
Numbl
Tcf4
THBS1
PDGFRA
MMP2
Pi3Kr1
Integrin
Gli3
G
HC
Scnn1a
Atp1a2
Ace
Setbp1
Tmbim1
Fam171a1
Gda
Ldhd
Cldn8
Duox2
Stk39
Rnf144b
AU021092
Aox3
Pcsk6
Kif12
H2-T23
Aqp5
Diff. expressed
DOWN
NO
UP
-log10(padj)
log2FoldChange
H
KHC
Pcsk6
Aqp5
Scnn1a
Aox1
Dclk1
Bicc1
Itpr2
Chgb
Duox2
Myrf
Clip4
Kif12
Atp2b1
Cbr2
Tshz1
diffexpressed
DOWN
NO
UP
-log10(padj)
log2FoldChange
I
Aqp5
p=4.5x10e-12
p=3.3x10e-67
Scnn1a
p=4.1x10e-33
p=1.9x10e-58
Pcsk6
p=1.1004 e-12
p=2.1161 e-116
Count normDESq2 of target gene
H
HC
KHC

Figure 5: Transcriptomic effects in HC and KHC pancreatic ductal organoids and associated ductal cell dysfunction

(A) Schematic representation of the generation of pancreatic ductal organoids from 12-week-old H, HC, and KHC mice, including pancreatic digestion with collagenase, manual sorting of ductal cells and culture in a BME2 dome for 7 days (created with Biorender). (B) Bright field and green fluorescence images of organoids from H, HC, and KHC mice on day 7. Scale bar, 50 µm. (C) Principal component analysis (PCA) of gene expression data across H (red squares, n=5), HC (blue dots, n=4), and KHC (green triangles, n=4) samples. (D) Venn diagrams showing upregulated (left panel) versus downregulated (right panel) genes and their overlap across the following comparisons: HC vs H, KHC vs H, and KHC vs HC. (E) Boxplot showing the transcript levels of Hnf1b in HC and KHC ducts compared with H ducts. (F) K-means heatmap showing clustering of H, HC, and KHC groups, highlighting clusters of downregulated pathways (blue), clusters of upregulated pathways (yellow, purple, green), and examples of associated genes, in HC and KHC compared with control H. (G) Volcano plot, with upregulated genes in blue and downregulated genes in red. Differential gene expression in HC compared with H. (H) Differential gene expression in KHC compared with H. (I) Boxplot showing the upregulation of Aqp5, Scnn1a, and Pcsk6 in HC and KHC compared with H.

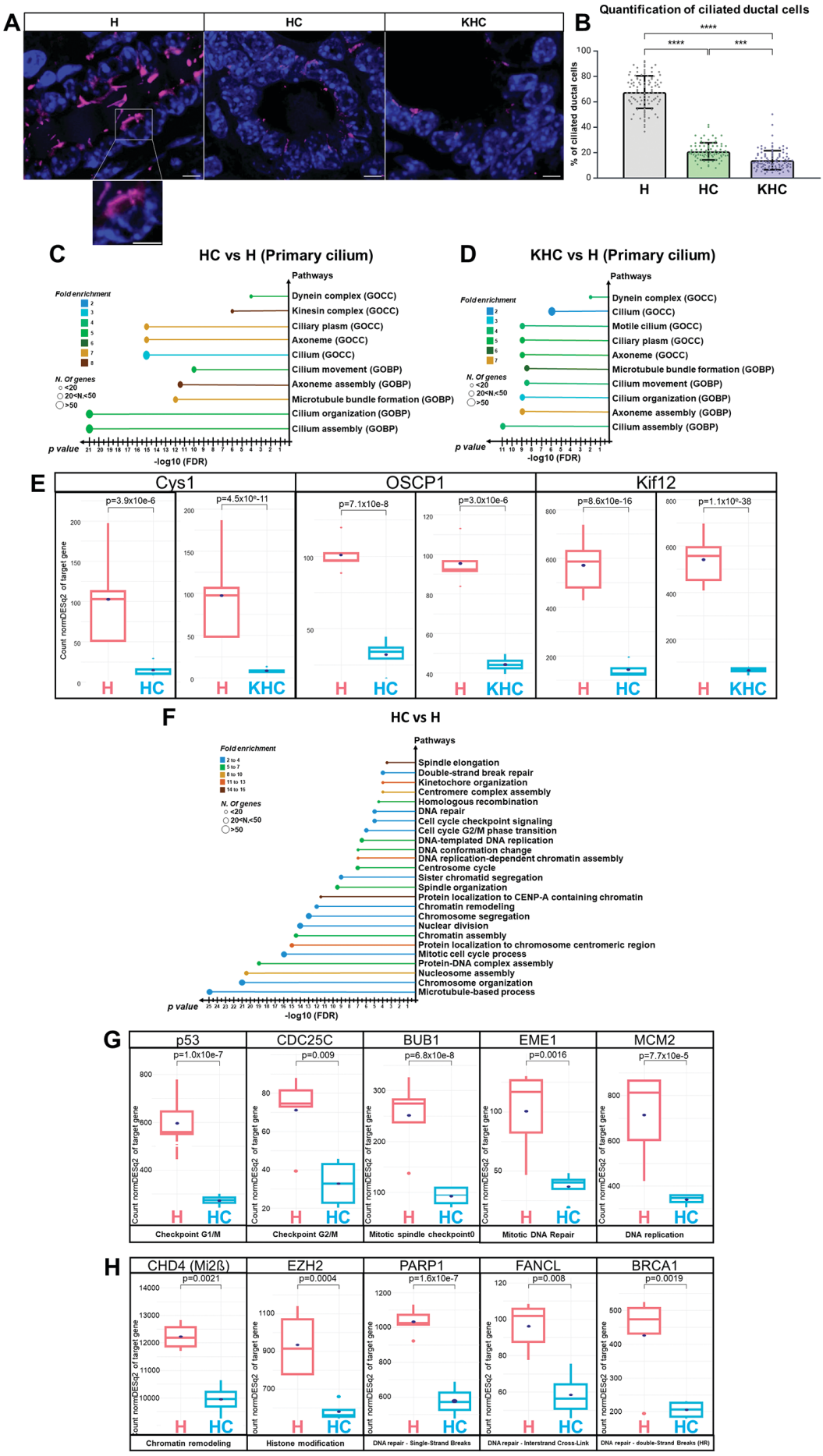
A
H
HC
KHC
B
Quantification of ciliated ductal cells
% of ciliated ductal cells
****
****
***
H
HC
KHC
C
HC vs H (Primary cilium)
Pathways
Fold enrichment
N. Of genes
<20
20<N.<50
>50
Dynein complex (GOCC)
Kinesin complex (GOCC)
Ciliary plasm (GOCC)
Axoneme (GOCC)
Cilium (GOCC)
Cilium movement (GOBP)
Axoneme assembly (GOBP)
Microtubule bundle formation (GOBP)
Cilium organization (GOBP)
Cilium assembly (GOBP)
p value
-log10 (FDR)
D
KHC vs H (Primary cilium)
Pathways
Fold enrichment
N. Of genes
<20
20<N.<50
>50
Dynein complex (GOCC)
Cilium (GOCC)
Motile cilium (GOCC)
Ciliary plasm (GOCC)
Axoneme (GOCC)
Microtubule bundle formation (GOBP)
Cilium movement (GOBP)
Cilium organization (GOBP)
Axoneme assembly (GOBP)
Cilium assembly (GOBP)
p value
-log10 (FDR)
E
Cys1
p=3.9x10e-6
p=4.5x10e-11
OSCP1
p=7.1x10e-8
p=3.0x10e-6
Kif12
p=8.6x10e-16
p=1.1x10e-38
Count normDESq2 of target gene
H
HC
KHC
F
HC vs H
Pathways
Fold enrichment
2 to 4
5 to 7
8 to 10
11 to 13
14 to 16
N. Of genes
<20
20<N.<50
>50
Spindle elongation
Double-strand break repair
Kinetochore organization
Centromere complex assembly
Homologous recombination
DNA repair
Cell cycle checkpoint signaling
Cell cycle G2/M phase transition
DNA-templated DNA replication
DNA conformation change
DNA replication-dependent chromatin assembly
Centrosome cycle
Sister chromatid segregation
Spindle organization
Protein localization to CENP-A containing chromatin
Chromatin remodeling
Chromosome segregation
Nuclear division
Chromatin assembly
Protein localization to chromosome centromeric region
Mitotic cell cycle process
Protein-DNA complex assembly
Nucleosome assembly
Chromosome organization
Microtubule-based process
p value
-log10 (FDR)
G
p53
p=1.0x10e-7
CDC25C
p=0.009
BUB1
p=6.8x10e-8
EME1
p=0.0016
MCM2
p=7.7x10e-5
Count normDESq2 of target gene
H
HC
Checkpoint G1/M
Checkpoint G2/M
Mitotic spindle checkpoint0
Mitotic DNA Repair
DNA replication
H
CHD4 (Mi2ß)
p=0.0021
EZH2
p=0.0004
PARP1
p=1.6x10e-7
FANCL
p=0.008
BRCA1
p=0.0019
Count normDESq2 of target gene
H
HC
Chromatin remodeling
Histone modification
DNA repair - Single-Strand Breaks
DNA repair - Interstrand Cross-Link
DNA repair - double-Strand Breaks (HR)

Figure 6: Downregulation of primary cilia-related pathways in HC and KHC, and downregulation of cell cycle/genomic stability regulatory pathways in HC compared with H

(A) Immunostaining of acetylated-tubulin (red) showing primary cilia loss in HC and KHC ductal cells. Nuclei are stained with Hoechst. Scale bar: 5 μm. (B) Quantification of ciliated ductal cells. (C-D) Lollipop diagrams of the Gene Ontology Biological Process (GOBP) and Gene Ontology Cellular Component (GOCC) pathways related to primary cilia, showing downregulation in HC and KHC ductal cells compared with control H. Each lollipop represents a pathway, with the x-axis indicating the -log10 of the p-value, reflecting the statistical significance of the downregulation, and the y-axis listing the pathway names. The color of the lollipops corresponds to the fold enrichment, with blue indicating lower enrichment and brown indicating higher enrichment. The size of the lollipop dots represents the number of genes involved in each pathway. (E) Boxplots illustrating the downregulation of genes associated with primary cilia (Cys1, Oscp1, Kif12) in HC and KHC ductal cells compared with control H. (F) Lollipop diagram of downregulated GOBP pathways involved in cell cycle regulation and genomic stability (DNA repair pathways, mitotic spindle, regulation of chromatin structure and function, cell division and its checkpoints) in HC compared with control H. (G, H). Boxplots showing the downregulation of key genes involved in pathways related to (G) cell cycle regulation and (H) genomic stability.

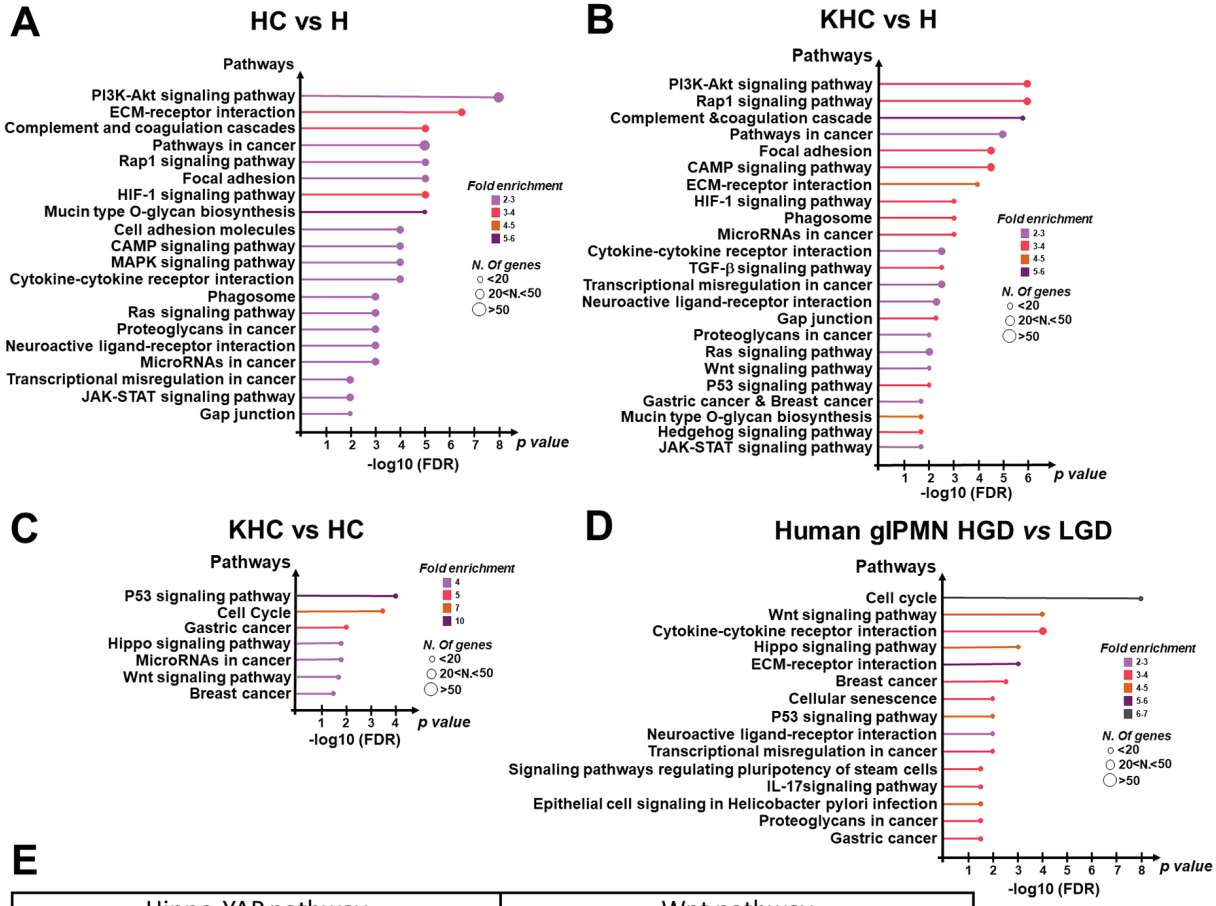
A
HC vs H
Pathways
PI3K-Akt signaling pathway
ECM-receptor interaction
Complement and coagulation cascades
Pathways in cancer
Rap1 signaling pathway
Focal adhesion
HIF-1 signaling pathway
Mucin type O-glycan biosynthesis
Cell adhesion molecules
CAMP signaling pathway
MAPK signaling pathway
Cytokine-cytokine receptor interaction
Phagosome
Ras signaling pathway
Proteoglycans in cancer
Neuroactive ligand-receptor interaction
MicroRNAs in cancer
Transcriptional misregulation in cancer
JAK-STAT signaling pathway
Gap junction
Fold enrichment
2-3
3-4
4-5
5-6
N. Of genes
<20
20<N.<50
>50
1 2 3 4 5 6 7 8
p value
-log10 (FDR)
B
KHC vs H
Pathways
PI3K-Akt signaling pathway
Rap1 signaling pathway
Complement &coagulation cascade
Pathways in cancer
Focal adhesion
CAMP signaling pathway
ECM-receptor interaction
HIF-1 signaling pathway
Phagosome
MicroRNAs in cancer
Cytokine-cytokine receptor interaction
TGF-β signaling pathway
Transcriptional misregulation in cancer
Neuroactive ligand-receptor interaction
Gap junction
Proteoglycans in cancer
Ras signaling pathway
Wnt signaling pathway
P53 signaling pathway
Gastric cancer & Breast cancer
Mucin type O-glycan biosynthesis
Hedgehog signaling pathway
JAK-STAT signaling pathway
Fold enrichment
2-3
3-4
4-5
5-6
N. Of genes
<20
20<N.<50
>50
1 2 3 4 5 6
p value
-log10 (FDR)
C
KHC vs HC
Pathways
P53 signaling pathway
Cell Cycle
Gastric cancer
Hippo signaling pathway
MicroRNAs in cancer
Wnt signaling pathway
Breast cancer
Fold enrichment
4
5
7
10
N. Of genes
<20
20<N.<50
>50
1 2 3 4
p value
-log10 (FDR)
D
Human gIPMN HGD vs LGD
Pathways
Cell cycle
Wnt signaling pathway
Cytokine-cytokine receptor interaction
Hippo signaling pathway
ECM-receptor interaction
Breast cancer
Cellular senescence
P53 signaling pathway
Neuroactive ligand-receptor interaction
Transcriptional misregulation in cancer
Signaling pathways regulating pluripotency of steam cells
IL-17signaling pathway
Epithelial cell signaling in Helicobacter pylori infection
Proteoglycans in cancer
Gastric cancer
Fold enrichment
2-3
3-4
4-5
5-6
6-7
N. Of genes
<20
20<N.<50
>50
1 2 3 4 5 6 7 8
p value
-log10 (FDR)
E
Hippo-YAP pathway
CCN2 (CTGF)
Wnt pathway
LEF1
Count normDESq2 of target gene
p=0.00017
p=4.4x10e-32
p=0.0047
p= 3.3x10e-6
p= 0.0013
p= 4.0x10e-5
H
HC
H
KHC
LGD
HGD
H
HC
H
KHC
LGD
HGD
F
G

Figure 7: Upregulated signaling pathways in IPMN initiation and progression in mice and humans, and increased IPMN prevalence in HNF1B patients

(A) Lollipop diagram of upregulated KEGG pathways in HC compared with H. (B) Lollipop diagram of upregulated KEGG pathways in KHC compared with H. (C) Lollipop diagram of upregulated KEGG pathways in KHC compared with HC. (D) Lollipop diagram of upregulated KEGG pathways in human gastric (g)IPMN, HGD compared with LGD. (E) Boxplots showing the upregulation of genes encoding effectors associated with the Hippo-YAP (CTGF/CCN2), Wnt (LEF1) and Notch (Notch3) pathways in HC and KHC compared with H controls; and in human gIPMN, HGD compared with LGD. (F, G) Axial T2-weighted MR image showing branch-duct IPMN in the pancreatic head of 2 young patients with a heterozygous germline mutation in HNF1B. The connection to the main pancreatic duct is clearly visible in (F), and mucus droplets are distinctly visible in (G).